Interlayer Pairing Induced Partially Gapped Fermi Surface in Trilayer $La_4Ni_3O_{10}$ Superconductors

Junkang Huang and Tao Zhou[*]

Guangdong Provincial Key Laboratory of Quantum Engineering and Quantum Materials,
School of Physics, Guangdong-Hong Kong Joint Laboratory of Quantum Matter,
and Frontier Research Institute for Physics, South China Normal University, Guangzhou 510006, China
(Dated: April 16, 2024)

We explore the superconducting pairing mechanisms in the trilayer $La_4Ni_3O_{10}$ material through self-consistent mean-field calculations. Our findings demonstrate that intralayer pairings are substantially weaker compared to interlayer ones. Remarkably, in the state characterized by interlayer pairing, we detect the presence of partially gapped Fermi surfaces, a fascinating occurrence attributable to the disparity between the inner and outer conducting layers of $La_4Ni_3O_{10}$. Moreover, this study provides valuable insights into the lower superconducting transition temperatures observed in $La_4Ni_3O_{10}$ compounds. This contributes to a deeper understanding of its distinct superconducting attributes.

The discovery of high-temperature bilayer nickelate superconductors, $La_3Ni_2O_7$, exhibiting a superconducting transition temperature (T_c) of 80 K under pressure, has garnered significant attention [1]. In the domain of cuprate-based high-T_c superconductors, there exists a wide variety of compounds, with trilayer structures achieving the highest superconducting transition temperatures [2, 3]. This paves the way for the investigation of novel layered nickelate materials that can support high-T_c superconductivity. The potential for superconductivity within trilayer nickelate $La_4Ni_3O_{10}$ was first explored by Sakakibara *et al.*, who postulated superconductivity based on density functional theory and fluctuation exchange approximation calculations [4].

Subsequently, the presence of superconductivity in $La_4Ni_3O_{10}$ was confirmed by various research groups, demonstrating T_c values within the range of $20-30$ K [5–8]. Notably, $La_4Ni_3O_{10}$ transitions from a monoclinic $P2_1/a$ space group to a tetragonal $I4/mmm$ space group under pressure [8], a transformation similarly observed in $La_3Ni_2O_7$ and considered crucial for the emergence of high-temperature superconductivity [1]. The electronic structures of these compounds exhibit notable similarities, with the Ni-d_{z^2} and Ni-$d_{x^2-y^2}$ orbitals primarily defining the Fermi level, leading to qualitatively similar Fermi surfaces [9–18]. However, unlike the cuprate family, the T_c of the trilayer nickelate $La_4Ni_3O_{10}$ is significantly lower than that of its bilayer counterpart, $La_3Ni_2O_7$.

Comprehensive theoretical and experimental studies have been conducted on $La_3Ni_2O_7$ and $La_4Ni_3O_{10}$. A critical question concerns the nature of interactions responsible for superconductivity. It has been proposed that, unlike conventional layered superconductors where pairing predominantly occurs within the layers, in $La_3Ni_2O_7$, strong interlayer hopping of d_{z^2} orbitals suggests that interlayer interactions might significantly influence pairing. Consequently, the dynamics between intra- and interlayer pairing has become a focal point [19–44], with some studies suggesting that interlayer pairing plays a dominant role in superconductivity [26–31], enhanced by significant Hund's coupling and fostering substantial interlayer interactions [27, 28, 44–46]. Experimental results from neutron scattering and resonant inelastic X-ray scattering further imply that magnetic superexchange interactions between layers considerably exceed those within layers. [47, 48]. Recent interest in the material $La_4Ni_3O_{10}$ has been largely focused on its pairing mechanism and symmetry [11–18]. Despite this attention, the intricate relationship and competition between interlayer and intralayer interactions are yet to be fully explored. Investigating these aspects could clarify the nuances of its superconducting properties and potentially highlight paths to enhance its performance.

The notable decrease in T_c for the trilayer compound has generated theoretical scrutiny. The proposed explanations include diminished electronic correlation in $La_4Ni_3O_{10}$ due to increased hole doping [14], a reduced pairing eigenvalue linked to weak antiferromagnetic exchange between the top and bottom layers [17, 18], and interlayer spin antiferromagnetic exchange catalyzed by interlayer hopping [49]. Notably, in multi-layer cuprate-based superconducting materials, T_c significantly increases with the layer count up to three and then gradually declines [2, 3]. This distinct difference between nickelates and cuprates offers an intriguing insight and could be crucial in understanding the nature of superconductivity in layered nickelate materials.

In this paper, we explore the superconductivity of $La_4Ni_3O_{10}$ through a two-orbital trilayer tight-binding model and a self-consistent approach. Our numerical explorations reveal that interlayer pairings predominantly facilitate superconductivity, whereas intralayer pairing magnitudes are negligibly small. In the superconducting state, the normal state Fermi surfaces are incompletely gapped, leaving some segments/points ungapped. This manifestation of partial Fermi surfaces in the superconducting state is ascribed to the energy band discrepancies

between inner and outer layer quasiparticles, thereby offering a plausible explanation for the diminished T_c in the La4Ni3O10 material.

Our investigation begins with a two-orbital model situated on a trilayer square lattice, encapsulating both the tight-binding and interaction terms, formulated as,

$$H = -\sum_{l,l'} \sum_{ij\tau\tau'\sigma} t_{ij\tau\tau'}^{l,l'} c_{i\tau\sigma}^{l\dagger} c_{j\tau'\sigma}^{l'\dagger} + H_I. \quad (1)$$

Here l and l' represent the layer indices, while τ and τ' denote the orbital indices, and σ refers to the spin index. The tight-binding parameters $t_{ij\tau\tau'}^{l,l'}$ are obtained from Ref. [12]. H_I signifies the superconducting pairing term, detailed as $H_I = \sum_{l,l'} \sum_{ij\tau} V_{ij\tau}^{l,l'} (c_{i\tau\uparrow}^{l\dagger} c_{j\tau\downarrow}^{l'\dagger} c_{i\tau\uparrow}^{l} c_{j\tau\downarrow}^{l'} + c_{i\tau\downarrow}^{l\dagger} c_{j\tau\uparrow}^{l'\dagger} c_{i\tau\downarrow}^{l} c_{j\tau\uparrow}^{l'})$. The mean-field order parameters for intra- and interlayer pairings are defined as $\Delta_{ij\tau}^{l,l} = \frac{V_{ij\tau}^{l,l}}{2} \langle c_{i\tau\uparrow}^{l} c_{j\tau\downarrow}^{l} - c_{i\tau\downarrow}^{l} c_{j\tau\uparrow}^{l} \rangle$, $\Delta_{ii\tau}^{l,l'} = \frac{V_{ii\tau}^{l,l'}}{2} \langle c_{i\tau\uparrow}^{l} c_{i\tau\downarrow}^{l'} - c_{i\tau\downarrow}^{l} c_{i\tau\uparrow}^{l'} \rangle$, respectively.

Through Fourier transformation, the Hamiltonian can be expressed in momentum space as $H = \sum_{\mathbf{k}} \Psi^{\dagger}(\mathbf{k}) \hat{M}(\mathbf{k}) \Psi(\mathbf{k})$, where the vector $\Psi(\mathbf{k}) = (u_{\mathbf{k}}, v_{\mathbf{k}})$ is given by

$$u_{\mathbf{k}} = \left(c_{\mathbf{k1}\uparrow}^{1}, c_{\mathbf{k2}\uparrow}^{1}, c_{\mathbf{k1}\uparrow}^{2}, c_{\mathbf{k2}\uparrow}^{2}, c_{\mathbf{k1}\uparrow}^{3}, c_{\mathbf{k2}\uparrow}^{3} \right)^{T},$$
$$v_{\mathbf{k}} = \left(c_{-\mathbf{k1}\downarrow}^{1\dagger}, c_{-\mathbf{k2}\downarrow}^{1\dagger}, c_{-\mathbf{k1}\downarrow}^{2\dagger}, c_{-\mathbf{k2}\downarrow}^{2\dagger}, c_{-\mathbf{k1}\downarrow}^{3\dagger}, c_{-\mathbf{k2}\downarrow}^{3\dagger} \right)^{T}, (2)$$

and $\hat{M}(\mathbf{k})$ is a 12×12 matrix.

The superconducting pairing terms include the intralayer channel and interlayer channel. Specifically, for intralayer attractions, we focus on nearest-neighbor interactions with $V_{\tau\parallel} = V_{ij\tau}^{l,l}$, representing the extended s-wave order parameters of the outer (O) (l=1,3) and inner (I) (l=2) layers. These are determined self-consistently as,

$$\Delta_{\tau}^{O(I)} = \frac{V_{\tau\parallel}}{4N} \sum_{n\mathbf{k}} (\cos \mathbf{k_x} + \cos \mathbf{k_y}) u_{\tau n\mathbf{k}}^{O(I)*} v_{\tau n\mathbf{k}}^{O(I)} \tanh \frac{\beta E_{n\mathbf{k}}}{2}.(3)$$

For the interlayer interaction, characterized by the interlayer interaction parameter $V_{\tau\perp} = V_{ii\tau}^{l,l+1}$, the order parameters $\Delta_{\tau\perp}$ are similarly determined,

$$\Delta_{\tau\perp} = \frac{V_{\tau\perp}}{2N} \sum_{n\mathbf{k}} u_{\tau n\mathbf{k}}^{O*} v_{\tau n\mathbf{k}}^{I} \tanh \frac{\beta E_{n\mathbf{k}}}{2}, \quad (4)$$

where $E_{n\mathbf{k}}$ denotes the eigenvalues of $\hat{M}(\mathbf{k})$ and $\beta = 10^{-5}$.

The spectral function, a crucial quantity for probing the electronic structure, is computed as,

$$A(\mathbf{k}, \omega) = -\frac{\text{Im}}{\pi} \sum_{p=1}^{6} \sum_{n} \frac{|u_{p,n\mathbf{k}}|^2}{\omega - E_{n\mathbf{k}} + i\Gamma} + \frac{|v_{p,n\mathbf{k}}|^2}{\omega + E_{n\mathbf{k}} + i\Gamma},(5)$$

with a damping factor $\Gamma = 0.002$.

Lastly, the density of states is represented as a function of frequency via integration of the spectral function over all momenta,

$$\rho(\omega) = \frac{1}{N} \sum_{\mathbf{k}} A(\mathbf{k}, \omega). \quad (6)$$

We begin our discussion by exploring the underlying interactions responsible for superconductivity. At the microscopic level, superconducting pairing is attributed to superexchange interactions J with $J \approx 4t^2/U$. Consequently, the effective pairing strength V, is fundamentally related to the square of the hopping constant, denoted as $V \propto t^2$. Here, t represents the hopping constant, as defined in the Hamiltonian of Eq.(1), derived from density functional theory calculations specified by Ref. [12] for pressurized La4Ni3O10. The calculated interlayer hopping constant ($t_\perp$) for the d_{z^2} orbital is 0.738, while the intralayer hopping constants ($t_\parallel$) for the outer and inner layers of the $d_{x^2-y^2}$ orbital are 0.511 and 0.521, respectively. Hopping constants through other channels are significantly lesser in magnitude. Subsequently, we estimate the ratio of the intralayer to interlayer pairing strength as $V_{x\parallel}/V_{z\perp} \approx 0.5$.

We now study the competition of the interlayer pairing and intralayer pairing numerically. Fixing the interlayer pairing strength for the d_{z^2} orbital $V_{z\perp}$ at 0.8 for illustrative purposes, we utilize a self-consistent method (Eqs. [3, 4]) to derive the behavior of order parameters relative to the intralayer pairing strength, $V_{x\parallel}$. As we adjust $V_{x\parallel}$ from 0.4 to 0.8, Fig. 1(a) reveals that the order parameter associated with interlayer pairing is largely unaffected by variations in $V_{x\parallel}$, maintaining a consistently high value. Remarkably, at a ratio of $V_{x\parallel}/V_{z\perp} = 0.5$, the magnitudes of the intralayer order parameters for both layers diminish to nearly zero. Further increments in $V_{x\parallel}$ result in a slight increase in the intralayer order parameters; however, these remain significantly lower than the interlayer parameter, even as $V_{x\parallel}$ equals $V_{z\perp}$. This observed trend underscores the predominance of interlayer pairing in determining the superconductivity of La4Ni3O10, a conclusion strongly supported by our numerical simulations, which were specifically conducted under the presumption of a $V_{x\parallel}/V_{z\perp} \approx 0.5$ interlayer pairing ratio.
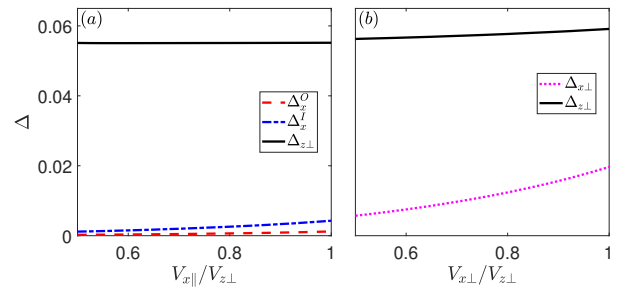

FIG. 1. Variation of order parameters with pairing potential from self-consistent calculations
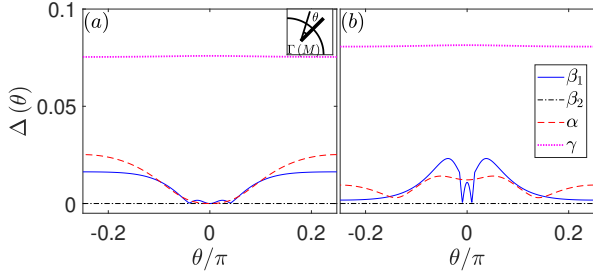
FIG. 2. Energy gap magnitudes along different Fermi pockets (a) without and (b) with interlayer $d_{x^2-y^2}$ orbital pairing.
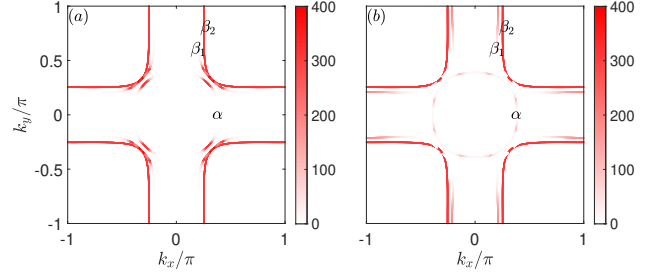

FIG. 3. Zero-energy spectral function spectra in the first Brillouin zone (a) without and (b) with interlayer $d_{x^2-y^2}$ orbital pairing.

The interlayer hopping constant for the $d_{x^2-y^2}$ orbital is notably small [12], essentially nullifying direct superexchange interactions for this orbital. Nevertheless, due to substantial Hund's coupling, the d_{z^2} orbital can endow the $d_{x^2-y^2}$ orbital with an interlayer pairing potential, thereby enabling interlayer pairing in the latter[27–31]. In this context, with the recognition of an effective interlayer pairing potential in the $d_{x^2-y^2}$ orbital ($V_{x\perp}$), our numerical analysis delineates the behavior of order parameters as a function of $V_{x\perp}$, which ranges from 0.4 to 0.8, as shown in Fig. 1(b). Remarkably, as $V_{x\perp}$ increases, not only is the pairing order parameter for the $d_{x^2-y^2}$ orbital initiated and bolstered, but there is also a slight elevation in the pairing order parameter of the d_{z^2} orbital. This observation suggests that the presence of Hund's coupling could potentially elevate the superconducting transition temperature.

The normal state Fermi surface of $La_4Ni_3O_{10}$ comprises four distinct Fermi pockets, namely γ, β_1, and β_2 pockets encircling the $M = (\pi, \pi)$ point of the Brillouin zone, and the α pocket encircling the $\Gamma = (0,0)$ point [12]. Our investigation explores the energy gaps along this normal state Fermi surface under the influence of interlayer pairing. The numerical results for two configurations, $(V_{x\perp}, V_{z\perp}) = (0, 0.8)$ and $(V_{x\perp}, V_{z\perp}) = (0.8, 0.8)$, are depicted in Fig. 2(a) and Fig. 2(b), respectively. With the absence of the $d_{x^2-y^2}$ orbital's pairing term, the most significant gap manifests along the γ Fermi pocket, attributable to the flat band proximal to the Fermi level within this band. The energy gaps across this pocket are nearly uniform. Remarkably, the β_2 Fermi surface exhibits no gaps. Conversely, the energy gaps demonstrated by the β_1 and α Fermi pockets show variability and display anisotropic properties, particularly, the gap magnitudes diminish to nearly zero in proximity to the diagonal direction and increase progressively as one moves away from this axis.

Upon the introduction of the pairing term for the $d_{x^2-y^2}$ orbital, key features broadly maintain qualitative similarity. The energy gaps along the γ Fermi pocket persist in being isotropic and exceedingly large, with slight increments in magnitude. The β_2 Fermi pocket continues exhibiting a gapless state. However, the anisotropic nature of the energy gaps around the β_1 and α Fermi pock-

ets evolve; with enhanced pairing in the $d_{x^2-y^2}$ orbital, distinctions in anisotropic behavior emerge. Notably, a minor gap appears precisely at the diagonal orientation ($\theta = 0$) of the β_1 Fermi pocket, with two nodal points positioned nearby. As θ extends, the energy gap escalates to its peak before diminishing with further increase in θ, ultimately approaching zero as it nears the off-diagonal position. Regarding the α Fermi surface, it becomes fully gapped, although the gap significantly reduces at certain intervals, demonstrating a nuanced modification induced by the addition of pairing in the $d_{x^2-y^2}$ orbital.

Details regarding the superconducting energy gap can be determined experimentally through techniques such as angle-resolved photoemission spectroscopy (ARPES) and scanning tunneling microscopy (STM). These experimental findings can be theoretically correlated by calculating the spectral function and the density of states. Intensity plots of zero energy spectral function spectra in the superconducting state, for configurations $(V_{x\perp}, V_{z\perp}) = (0, 0.8)$ and $(V_{x\perp}, V_{z\perp}) = (0.8, 0.8)$, are presented in Fig. 2(a) and 2(b), respectively.

The zero-energy spectral function is indicative of the distribution of zero-energy quasiparticles, typically found in the gapless regions of the Fermi surface. Around the γ Fermi pocket, the spectral function exhibits zero intensity, reflecting the large superconducting gap. Conversely, the entire β_2 Fermi pocket is characterized by its gapless nature, resulting in pronounced zero-energy spectral functions along this pocket. In the absence of pairing potential in the $d_{x^2-y^2}$ orbital, as shown in Fig. 2(a), the β_1 and α Fermi pockets exhibit partial gapping, with segments of the Fermi surface existing along the diagonal direction. With the introduction of pairing potential in the $d_{x^2-y^2}$ orbital, evidenced in Fig. 2(b), quasiparticles emerge at locations where energy gaps are minimal. Specifically, for the β_1 pocket, quasiparticles are observed near the Brillouin zone boundary. Although the α Fermi pocket is entirely gapped, minute energy gaps at certain locations result in a non-zero spectral function at these points.

We next examine the density of states spectra, also under two different configurations: $(V_{x\perp}, V_{z\perp}) = (0, 0.8)$ and $(V_{x\perp}, V_{z\perp}) = (0.8, 0.8)$. The numerical results are illustrated in Fig. 4. A notable peak in positive energy,
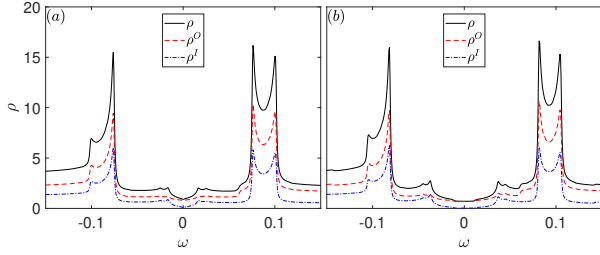
FIG. 4. Density of states (a) in the absence and (b) presence of interlayer $d_{x^2-y^2}$ orbital pairing.

FIG. 5. (a) Normal state Fermi surface of $La_4Ni_3O_{10}$, highlighted by layer contributions. (b) Modified Fermi surface depiction emphasizing orbital weight.

approximately at 0.1, originates from the van Hove singularity in the normal state energy bands. Additional peaks observed are attributable to superconducting coherence peaks, which arise from superconducting pairing.

Distinct two-gap features are evident within the spectra. The larger superconducting coherence peaks, associated with sizeable gaps, are primarily contributions from the γ Fermi pocket. Conversely, the β_1 Fermi pocket is responsible for the smaller energy gaps observed. The spectral weight associated with the α Fermi pocket is comparatively low, resulting in the absence of superconducting coherence peaks attributed to this pocket.

The introduction of pairing in the $d_{x^2-y^2}$ orbital markedly increases the maximum superconducting gap around the β_1 Fermi pocket, as detailed in Fig. 2. Consequently, the superconducting coherence peaks, primarily contributed by the β_1 Fermi pocket, also advance to higher energy levels.

Additionally, our numerical analyses suggest a contrasting behavior between the inner and outer layer density of states near the Fermi level. Specifically, the density of states approaches zero at the Fermi level within the inner layer, yet remains finite at low energies in the outer layer. This implies that zero-energy quasiparticles in the superconducting state are predominantly localized in the outer layer.

The phenomenon of a partially gapless Fermi surface can be coherently explained through the Fermiology inherent to the system. The $La_4Ni_3O_{10}$ compound is structured with three NiO_2 layers within its unit cell, where the outer and inner layers are distinct from each other. Consequently, in the normal state, the distribution of quasiparticles at the Fermi level differs between the outer and inner layers. In the transition to the superconducting state, where pairing occurs between the inner and outer layers, a natural consequence is the inability of some quasiparticles at the Fermi level to pair, resulting in a partially gapless Fermi surface. For a clearer understanding, we have illustrated the normal state Fermi surface in Fig. 5, with color bars in Fig. 5(a) and 5(b) indicating the contributions from the respective layers and orbitals to the Fermi surface. As demonstrated in Fig. 5(a), the β_2 Fermi pocket is entirely a result of the outer layer contribution, rendering it ungappable in the superconducting state. Conversely, as shown in Fig. 5(b), the
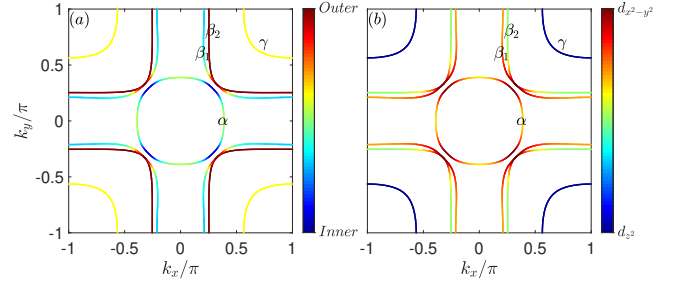
β_1 and α Fermi pockets primarily derive from the $d_{x^2-y^2}$ orbital. Notably, along the diagonal direction, the contribution from the $d_{x^2-y^2}$ orbital reaches its maximum. Hence, in the absence of pairing within the $d_{x^2-y^2}$ orbital, the β_1 and α Fermi pockets remain gapless along the diagonal direction. The introduction of interlayer pairing within the $d_{x^2-y^2}$ orbital significantly influences the energy gaps of these pockets, with the gap magnitudes strongly correlated to the contribution weight of the $d_{x^2-y^2}$ orbital.

The observed significant reduction in the superconducting transition temperature T_c of $La_4Ni_3O_{10}$ compared to $La_3Ni_2O_7$ can be attributed to the distinct layer configurations and their contribution to superconductivity. Specifically, in $La_4Ni_3O_{10}$, the non-equivalence of the inner and outer layers means that only a subset of the quasiparticles at the Fermi level engage in superconductivity within an interlayer pairing framework. In contrast, the bilayer La_3Ni2O_7 features two equivalent NiO_2 layers, enabling all quasiparticles at the Fermi level to participate in superconductivity, thus resulting in a higher T_c. This conceptual framework is supported by numerical analyses; using the same pairing interaction as in our study, the order parameter in bilayer samples is roughly twice that observed in our current findings. Given that the magnitude of the superconducting gap is directly proportional to T_c at the mean field level, this approach effectively explains the observed differences in T_c between the bilayer and trilayer nickelate superconductors.

To deepen our understanding, a comparative examination of multilayer cuprate and nickelate superconductors is essential. In cuprate superconductors, the $d_{x^2-y^2}$ orbital plays a pivotal role in fostering intralayer superconducting pairing. For multilayer samples, it was proposed that T_c can significantly increase as a result of superconducting pairing tunneling between layers [50]. Consequently, for a trilayer sample, a considerable elevation in T_c is observed [2, 3]. It is important to highlight, however, that for samples with four or more layers, T_c tends to decrease gradually, a phenomenon attributed to inhomogeneous charge distribution[2]. In stark contrast, superconductivity in nickelate materials is predominantly

reliant on interlayer pairing, with pairing tunneling playing no practical role. Thus, for multilayer nickelates, increasing the number of layers does not correlate with an increase in T_c.

In summary, our mean-field level analyses, complemented by self-consistent calculations, lead us to conclude that interlayer pairing mechanisms are responsible for the superconductivity observed in trilayer $La_4Ni_3O_{10}$ material. In the superconducting state, the Fermi surface exhibits partially gapped pockets. The presence of gapless Fermi surface segments can be attributed to the asymmetry between the inner and outer NiO_2 layers. This framework also provides a plausible explanation for the observed decrease in the superconducting transition temperature of $La_4Ni_3O_{10}$.

[1] H. Sun, M. Huo, X. Hu, J. Li, Z. Liu, Y. Han, L. Tang, Z. Mao, P. Yang, B. Wang, J. Cheng, D.-X. Yao, G.-M. Zhang, and M. Wang, Signatures of superconductivity near 80 in a nickelate under high pressure, Nature **621**, 493 (2023).

[2] M. Di Stasio, K. A. Müller, and L. Pietronero, Nonhomogeneous charge distribution in layered high-t_c superconductors, Phys. Rev. Lett. **64**, 2827 (1990).

[3] G. Sun, K. Wong, B. Xu, Y. Xin, and D. Lu, Tc enhancement of hgba2ca2cu3o8+未 by tl substitution, Physics Letters A **192**, 122 (1994).

[4] H. Sakakibara, M. Ochi, H. Nagata, Y. Ueki, H. Sakurai, R. Matsumoto, K. Terashima, K. Hirose, H. Ohta, M. Kato, Y. Takano, and K. Kuroki, Theoretical analysis on the possibility of superconductivity in a trilayer ruddlesden-popper nickelate la4ni3o10 under pressure and its experimental examination: comparison with la3ni2o7 (2023), arXiv:2309.09462 [cond-mat.supr-con].

[5] Q. Li, Y.-J. Zhang, Z.-N. Xiang, Y. Zhang, X. Zhu, and H.-H. Wen, Signature of superconductivity in pressurized la4ni3o10, Chin. Phys. Lett. **41**, 017401 (2024).

[6] Y. Zhu, E. Zhang, B. Pan, X. Chen, D. Peng, L. Chen, H. Ren, F. Liu, N. Li, Z. Xing, J. Han, J. Wang, D. Jia, H. Wo, Y. Gu, Y. Gu, L. Ji, W. Wang, H. Gou, Y. Shen, T. Ying, X. Chen, W. Yang, C. Zheng, Q. Zeng, J. gang Guo, and J. Zhao, Superconductivity in trilayer nickelate la4ni3o10 single crystals (2024), arXiv:2311.07353 [cond-mat.supr-con].

[7] M. Zhang, C. Pei, X. Du, W. Hu, Y. Cao, Q. Wang, J. Wu, Y. Li, H. Liu, C. Wen, Y. Zhao, C. Li, W. Cao, S. Zhu, Q. Zhang, N. Yu, P. Cheng, L. Zhang, Z. Li, J. Zhao, Y. Chen, H. Guo, C. Wu, F. Yang, S. Yan, L. Yang, and Y. Qi, Superconductivity in trilayer nickelate la4ni3o10 under pressure (2024), arXiv:2311.07423 [cond-mat.supr-con].

[8] J. Li, C.-Q. Chen, C. Huang, Y. Han, M. Huo, X. Huang, P. Ma, Z. Qiu, J. Chen, X. Hu, L. Chen, T. Xie, B. Shen, H. Sun, D.-X. Yao, and M. Wang, Structural transition, electric transport, and electronic structures in the compressed trilayer nickelate la4ni3o10, Sci. Chi. Phys. Mech. Astron. **67**, 117403 (2024).

[9] Z. Luo, X. Hu, M. Wang, W. Wú, and D.-X. Yao, Bilayer two-orbital model of $La_3Ni_2O_7$ under pressure, Phys. Rev. Lett. **131**, 126001 (2023).

[10] V. Christiansson, F. Petocchi, and P. Werner, Correlated electronic structure of la3ni2o7 under pressure, Phys. Rev. Lett. **131**, 206501 (2023).

[11] I. V. Leonov, Electronic structure and magnetic correlations in trilayer nickelate superconductor la4ni3o10 under pressure (2024), arXiv:2401.07350 [cond-mat.str-el].

[12] Z. Luo, C.-Q. Chen, M. Wang, W. W煤, and D.-X. Yao, Trilayer multi-orbital models of $La_4Ni_3O_{10}$ (2024), arXiv:2402.07196 [cond-mat.supr-con].

[13] P.-F. Tian, H.-T. Ma, X. Ming, X.-J. Zheng, and H. Li, Effective model and electron correlations in trilayer nickelate superconductor la4ni3o10 (2024), arXiv:2402.02351 [cond-mat.str-el].

[14] J.-X. Wang, Z. Ouyang, R.-Q. He, and Z.-Y. Lu, Non-fermi liquid and hund correlation in la4ni3o10 under high pressure (2024), arXiv:2402.02581 [cond-mat.str-el].

[15] H. LaBollita, J. Kapeghian, M. R. Norman, and A. S. Botana, Electronic structure and magnetic tendencies of trilayer la4ni3o10 under pressure: structural transition, molecular orbitals, and layer differentiation (2024), arXiv:2402.05085 [cond-mat.supr-con].

[16] Y. Zhang, L.-F. Lin, A. Moreo, T. A. Maier, and E. Dagotto, Prediction of $s^{\pm}$-wave superconductivity enhanced by electronic doping in trilayer nickelates la4ni3o10 under pressure (2024), arXiv:2402.05285 [cond-mat.supr-con].

[17] Q.-G. Yang, K.-Y. Jiang, D. Wang, H.-Y. Lu, and Q.-H. Wang, Effective model and $s_{\pm}$-wave superconductivity in trilayer nickelate la4ni3o10 (2024), arXiv:2402.05447 [cond-mat.supr-con].

[18] M. Zhang, H. Sun, Y.-B. Liu, Q. Liu, W.-Q. Chen, and F. Yang, The $s^{\pm}$-wave superconductivity in the pressurized la4ni3o10 (2024), arXiv:2402.07902 [cond-mat.supr-con].

[19] Y. Gu, C. Le, Z. Yang, X. Wu, and J. Hu, Effective model and pairing tendency in bilayer ni-based superconductor la3ni2o7 (2023), arXiv:2306.07275 [cond-mat.supr-con].

[20] W. Wu, Z. Luo, D.-X. Yao, and M. Wang, Superexchange and charge transfer in the nickelate superconductor la3ni2o7 under pressure, Sci. Chi. Phys. Mech. Astron. **67**, 117402 (2024).

[21] Y. Shen, M. Qin, and G.-M. Zhang, Effective bi-layer model hamiltonian and density-matrix renormalization group study for the high-tc superconductivity in la3ni2o7 under high pressure, Chin. Phys. Lett. **40**, 127401 (2023).

[22] Q. Qin and Y.-f. Yang, High-T_c superconductivity by mobilizing local spin singlets and possible route to higher T_c in pressurized la3ni2o7, Phys. Rev. B **108**, L140504 (2023).

[23] D.-C. Lu, M. Li, Z.-Y. Zeng, W. Hou, J. Wang, F. Yang, and Y.-Z. You, Superconductivity from doping symmetric mass generation insulators: Application to la3ni2o7 under pressure (2023),

arXiv:2308.11195 [cond-mat.str-el].

[24] H. Lange, L. Homeier, E. Demler, U. Schollwock, A. Bohrdt, and F. Grusdt, Pairing dome from an emergent feshbach resonance in a strongly repulsive bilayer model (2024), arXiv:2309.13040 [cond-mat.str-el].

[25] H. Schlomer, U. Schollwock, F. Grusdt, and A. Bohrdt, Superconductivity in the pressurized nickelate $la_3ni_2o_7$ in the vicinity of a bec-bcs crossover (2023), arXiv:2311.03349 [cond-mat.str-el].

[26] Y.-f. Yang, G.-M. Zhang, and F.-C. Zhang, Interlayer valence bonds and two-component theory for high-T_c superconductivity of $la_3ni_2o_7$ under pressure, Phys. Rev. B **108**, L201108 (2023).

[27] C. Lu, Z. Pan, F. Yang, and C. Wu, Interplay of two e_g orbitals in superconducting $la_3ni_2o_7$ under pressure (2023), arXiv:2310.02915 [cond-mat.supr-con].

[28] H. Oh and Y.-H. Zhang, Type-ii $t - j$ model and shared superexchange coupling from hund's rule in superconducting $la_3ni_2o_7$, Phys. Rev. B **108**, 174511 (2023).

[29] J. Chen, F. Yang, and W. Li, Orbital-selective superconductivity in the pressurized bilayer nickelate $la_3ni_2o_7$: An infinite projected entangled-pair state study (2023), arXiv:2311.05491 [cond-mat.str-el].

[30] C. Lu, Z. Pan, F. Yang, and C. Wu, Interlayer-coupling-driven high-temperature superconductivity in $la_3ni_2o_7$ under pressure, Phys. Rev. Lett. **132**, 146002 (2024).

[31] J.-R. Xue and F. Wang, Magnetism and superconductivity in the $t - j$ model of $la_3ni_2o_7$ under multiband gutzwiller approximation (2024), arXiv:2402.07449 [cond-mat.supr-con].

[32] Y. Zhang, L.-F. Lin, A. Moreo, T. A. Maier, and E. Dagotto, Trends in electronic structures and $s_\pm$-wave pairing for the rare-earth series in bilayer nickelate superconductor $R_3ni_2o_7$, Phys. Rev. B **108**, 165141 (2023).

[33] Y.-B. Liu, J.-W. Mei, F. Ye, W.-Q. Chen, and F. Yang, $s^\pm$-wave pairing and the destructive role of apical-oxygen deficiencies in $la_3ni_2o_7$ under pressure, Phys. Rev. Lett. **131**, 236002 (2023).

[34] X.-Z. Qu, D.-W. Qu, J. Chen, C. Wu, F. Yang, W. Li, and G. Su, Bilayer $t-J-J_\perp$ model and magnetically mediated pairing in the pressurized nickelate $la_3ni_2o_7$, Phys. Rev. Lett. **132**, 036502 (2024).

[35] Z. Fan, J.-F. Zhang, B. Zhan, D. Lv, X.-Y. Jiang, B. Normand, and T. Xiang, Superconductivity in nickelate and cuprate superconductors with strong bilayer coupling (2023), arXiv:2312.17064 [cond-mat.supr-con].

[36] J.-X. Zhang, H.-K. Zhang, Y.-Z. You, and Z.-Y. Weng, Strong pairing originated from an emergent Z_2 berry phase in $La_3Ni_2O_7$ (2023), arXiv:2309.05726 [cond-mat.str-el].

[37] H. Yang, H. Oh, and Y.-H. Zhang, Strong pairing from small fermi surface beyond weak coupling: Application to $la_3ni_2o_7$ (2023), arXiv:2309.15095 [cond-mat.str-el].

[38] H. Sakakibara, N. Kitamine, M. Ochi, and K. Kuroki, Possible high T_c superconductivity in $la_3ni_2o_7$ under high pressure through manifestation of a nearly half-filled bilayer hubbard model, Phys. Rev. Lett. **132**, 106002 (2024).

[39] J. Huang, Z. D. Wang, and T. Zhou, Impurity and vortex states in the bilayer high-temperature superconductor $la_3ni_2o_7$, Phys. Rev. B **108**, 174501 (2023).

[40] Y. Wang, K. Jiang, Z. Wang, F.-C. Zhang, and J. Hu, Electronic structure and superconductivity in bilayer $la_3ni_2o_7$ (2024), arXiv:2401.15097 [cond-mat.supr-con].

[41] Z. Luo, B. Lv, M. Wang, W. W煤, and D.-X. Yao, High-t_c superconductivity in $La_3Ni_2O_7$ based on the bilayer two-orbital t-j model (2023), arXiv:2308.16564 [cond-mat.supr-con].

[42] Z. Liao, L. Chen, G. Duan, Y. Wang, C. Liu, R. Yu, and Q. Si, Electron correlations and superconductivity in $la_3ni_2o_7$ under pressure tuning, Phys. Rev. B **108**, 214522 (2023).

[43] S. Ryee, N. Witt, and T. O. Wehling, Quenched pair breaking by interlayer correlations as a key to superconductivity in $la_3ni_2o_7$ (2024), arXiv:2310.17465 [cond-mat.supr-con].

[44] Y.-H. Tian, Y. Chen, J.-M. Wang, R.-Q. He, and Z.-Y. Lu, Correlation effects and concomitant two-orbital $s_\pm$-wave superconductivity in $la_3ni_2o_7$ under high pressure (2023), arXiv:2308.09698 [cond-mat.supr-con].

[45] Y. Cao and Y.-f. Yang, Flat bands promoted by hund's rule coupling in the candidate double-layer high-temperature superconductor $la_3ni_2o_7$ under high pressure, Phys. Rev. B **109**, L081105 (2024).

[46] X.-Z. Qu, D.-W. Qu, W. Li, and G. Su, Roles of hund's rule and hybridization in the two-orbital model for high-t_c superconductivity in the bilayer nickelate (2023), arXiv:2311.12769 [cond-mat.str-el].

[47] T. Xie, M. Huo, X. Ni, F. Shen, X. Huang, H. Sun, H. C. Walker, D. Adroja, D. Yu, B. Shen, L. He, K. Cao, and M. Wang, Neutron scattering studies on the high-t_c superconductor $la_3ni_2o_{7-\delta}$ at ambient pressure (2024), arXiv:2401.12635 [cond-mat.supr-con].

[48] X. Chen, J. Choi, Z. Jiang, J. Mei, K. Jiang, J. Li, S. Agrestini, M. Garcia-Fernandez, X. Huang, H. Sun, D. Shen, M. Wang, J. Hu, Y. Lu, K.-J. Zhou, and D. Feng, Electronic and magnetic excitations in $la_3ni_2o_7$ (2024), arXiv:2401.12657 [cond-mat.supr-con].

[49] C. Lu, Z. Pan, F. Yang, and C. Wu, Superconductivity in $la_4ni_3o_{10}$ under pressure (2024), arXiv:2402.06450 [cond-mat.supr-con].

[50] T. Zhou, Theoretical investigation of the four-layered self-doped high-T_c superconductors: Evidence of the pair tunneling effect, Phys. Rev. Lett. **106**, 167001 (2011).